Electronic Supplementary Material (ESI) for Journal of Materials Chemistry A.

Design of sepiolite-supported ionogel-embedded composite membranes without proton carrier wastage for wide-temperature-range operation of proton exchange membrane fuel cells

Xiaoxiao Zhang[a], Xudong Fu[a], Shoukun Yang[a], Yuanfang Zhang[a], Rong Zhang[a], Shengfei Hu[a], Xujin Bao[a, b, *], Feng Zhao[c], Xiao Li[c], Qingting Liu[a, *]

[a] Hubei Provincial Key Laboratory of Green Materials for Light Industry, School of Materials and Chemical Engineering, Hubei University of Technology, Wuhan, 430068, China

[b] Department of Materials, Loughborough University, Leicestershire, LE11 3TU, UK

[c] Wuhan Troowin Power System Technology Co., Ltd., Wuhan, 430079, China

* E-mail: liuqt@hbut.edu.cn (Q. Liu); X.Bao@lboro.ac.uk (X. Bao)

Supplementary materials

1. Experimental details

1.1 Microwave-assisted acid activation treatment of sepiolite

A laboratory microwave chemical reactor (Mobilelab, Tangshan Nyuan Microwave Thermal Instrument Manufacturing Co., Ltd., China) operating at 1.0 kW was used for acid activation treatment. The duration of microwave irradiation governs the intensity of the reaction. 100 mL of 2 M HCl was added to 10.0 g of sepiolite and irradiated by microwave at 80 °C for 0.5, 1, 1.5, 2, 2.5 h, respectively; then, the obtained suspensions were filtered and washed thoroughly with ethanol and plenty of deionized water (until the filtrates were neutral) and then dried at 110 °C for 24 h to obtain microwave-assisted acid activated sepiolite (marked as Sep–MW). The prepared samples are designated as Sep–MW0.5h to Sep–MW2.5h according to the time duration of microwave irradiation in the acid activation treatment.

1.2 Characterization of SNR and IL@SNR ionogel

The chemical and crystal structures of sepiolite particles before and after microwave-assisted acid activation and IL modification were characterized via FTIR (Tensor 2, Bruker, USA) with a resolution of 4 cm^{-1} and 64 scans in the region of 4000 cm^{-1}–400 cm^{-1}, XRD (Empyrean type XRD analyzer, PANalytical B.V., Netherlands) over a range of $5° \leq 2\theta \leq 50°$, using a Cu Kα X-ray source (40 kV, 40 mA). Raman spectra of powdered samples were performed on a laser confocal Raman spectroscopy (LabRam HR Evolution, HORIBA JOBIN YVON, France) with 532 nm exciting radiation. The surface composition and elements chemical valence was

analyzed by X-ray photoelectron spectra (XPS, PHI 5000 Versaprobe Ⅲ, ULVAC-PHI, Japan) with Al Kα radiation and the energy calibration was carried out using the C 1s peak of adventitious C at 284.6 eV.

The content of Mg^{2+} in sepiolite samples was determined via Inductively Coupled Plasma Emission Spectroscopy (ICP-OES) (Perkin Elmer, Optima 5300 DV, USA), and the removed Mg^{2+} was calculated with the following equations (removed Mg^{2+} (%)= (W_{Sep} - $W_{Sep–MW}$) / W_{Sep} × 100), where W_{Sep} represents the Mg^{2+} content in Sep and $W_{Sep–MW}$ represents the residual Mg^{2+} content in Sep–MW sample after microwave-assisted acid activation treatment.

The specific surface area and pore structure of nano-fibrous sepiolite were analyzed by N_2 adsorption-desorption isotherms (BELSORP-miniII, Japan McKike Bayer Co., Ltd., Japan) measured at -196 °C. Prior to the adsorption-desorption tests, samples were degassed at 150 °C for 24 h.

Morphological analysis was conducted via FESEM (SU801, Hitachi, Japan), TEM (Tecnai G2 20, FEI, USA), and atomic resolution high-angle annular dark-field with scanning electron probe STEM mode (HAADT-STEM, TecnaiG2 F20 S-TWIN, FEI, USA).

TGA was examined in a temperature range of 30 °C–800 °C under N_2 atmosphere at a heating rate of 10 °C/min with a thermal analyzer (SDT Q600, TA instruments, USA) to evaluate the thermal stabilities and thermodynamic behaviors of sepiolite particles before and after IL modification.

1.3 Characterization of ABPBI/IL@SNR composite membranes

Specifically, a FESEM (SU801, Hitachi, Japan) coupled with Energy Dispersive X-ray Spectroscope (EDS) and TEM (TF20，Jeol 2100F, Japan) was used to perform the membrane fracture surface characterization and distribution of elements. The samples were coated with a layer of gold prior to the measurement. The crystal structures of the membranes were characterized via XRD (Empyrean type XRD analyzer, PANalytical B.V., Netherlands) over a range of $5° \leq 2\theta \leq 30°$, using a Cu Kα X-ray source (40 kV, 40 mA). The mechanical properties of the membranes were obtained via DMA and tensile tests. DMA was conducted with a Q800 DMA (TA instruments, USA) at a heating rate of 3 °C/min from 25 to 300 °C at a sinusoidal frequency of 1 Hz and 0.1% strain. Tensile test was conducted with an Electronic Universal Testing Machine (CMT4204, Mester, China) at a tensile speed of 50 mm/min under ambient atmosphere. Each sample at the size of 10×2.5 mm is measured 5 times and then averaged was obtained. TGA was examined in a temperature range of 30 °C–800 °C under N_2 atmosphere at a heating rate of 10 °C/min with a thermal analyzer (SDT Q600, TA instruments, USA).

The oxidative stability of the membranes was evaluated via immersion in Fenton's reagent (3% H_2O_2 containing 4 ppm Fe^{2+}) for 5 d at 70 °C. Prior to dipping in Fenton's solution, the initial weight of the dried membranes was noted as W_0, and their weights were recorded as W_i (after drying at 110 °C in a vacuum oven) for every 24 h. Then, the membranes were re-immersed in the fresh Fenton's reagent. Their oxidative stability was measured as the remaining weight percentage after taking the

membranes out of Fenton's reagent.

The measurement and calculation for water uptake and PA DL of a membrane refer to previously published equations (Q. Liu, et al., *Int J Hydrogen Energ*, 2016, **41**, 16160-16166). The water uptake measurement was performed by putting dried membranes (dried at 110 °C in a vacuum oven for 24 h until they reached a constant weight) in deionized water at room temperature for 24 h. Acid retention, swelling ratio, and swelling volume measurements of ABPBI and ABPBI/IL@SNR composite membranes were conducted adapted from our previous work (X. Zhang, et al., *J Membrane Sci*, 2019, **574**, 282-298). All membranes were first dried completely in a vacuum oven at 110 °C for 24 h and their weights and dimensions in *x*, *y*, and *z* directions were noted. The PA-doped membranes were repeatedly rinsed with deionized water and then mopped with filter paper to remove water and PA on the surface; then, their weights (W_0) and dimensions were measured again. The swelling ratio of area and volume were calculated using the following equations (swelling area $\Delta S = (S_w - S_d) / S_d \times 100\ \%$, $S = x \times y$; swelling volume $\Delta V = (V_w - V_d) / V_d \times 100\ \%$, $V = x \times y \times z$), where S_d and S_w is the area of the dry and wet membranes, respectively; V_d and V_w is the volume of the dry and wet membranes, respectively. They were then hanged over boiling water for 5 h and the weights of the membranes (W_i) were measured every 20 min during the first hour and then every 60 min after wiping off the acid that leached from the membranes. The weight loss ratio of PA in the membranes was calculated using the formula (weight loss ratio $R = (W_0 - W_i) / W_a$), Where, W_0 represents the initial weight of the PA doped membranes, W_i represents the

weight of the membranes after each hour of leaching, and W_a represents the original weight of PA present in the membranes calculated from PA DL measurements.

The impedance spectra were obtained via a two-electrode AC impedance spectroscopy (PARSTAT 4000, Princeton, USA) and an environmental test chamber (LP-80U, Guangdong Hongzhan tech, China). The impedance spectra were recorded from 4 MHz to 1 Hz. The through-plane proton conductivity (σ) was calculated from the measured current resistance (R) using the equation ($\sigma = L / (R \times A)$), where, σ, L, R, and A, represent proton conductivity (S/cm), distance between two electrodes, i.e. membrane thickness (cm) in this case, resistance from the impedance data (Ω), and cross-sectional area (cm^2) of the membranes, respectively.

Gas diffusion layer (carbon paper, Avcarb GDS2240) incorporated with wet proofed micro-porous layer (H2315 T10AC1) obtained from Freudenburg (FFCCT, Germany) was used as substrate with size of 1 cm^2 to deposit the catalyst layer for the electrode. The catalyst inks were prepared by blending catalysts (20 wt% Pt/C, Alfa Aesar) in a water/ethanol mixture and ultrasonic vibrated for 1 h. Then, the catalyst inks were sprayed onto carbon substrate at 100 °C, and the electrodes were held at 150 °C for 2 h to remove residual solvent. The Pt loadings on the cathode and anode were both 0.4 mg/cm^2. The membrane electrode assembly (MEA) was finally obtained by hot pressing the electrodes onto PA doped membranes at 5 MPa for 3 min at 120 °C. Dry H_2 and O_2 were fed into the cell at flow rates of both 200 cm^3/min. To ensure the steady state, the cell was held at each desired conditions for 1 h before performing the measurements.

2. Results

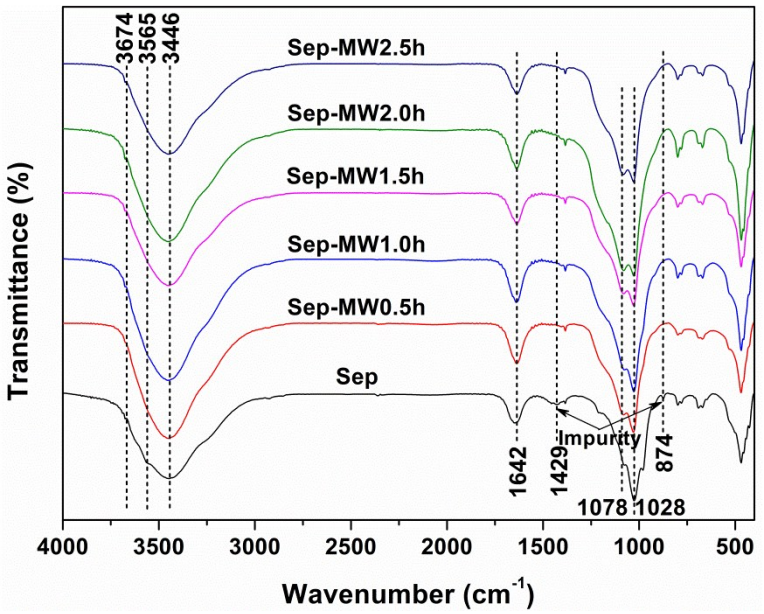

Fig. S1 FTIR spectra of Sep and Sep–MW.

In Fig. S1, the O–H stretching vibration from the octahedral sheet and Mg_3OH in the external surface of sepiolite appeared at 3674 and 3565 cm^{-1}, respectively. The bands at 3446 and 1642 cm^{-1} are correspond to O–H stretching vibration and bending vibration of coordinated H_2O (the zeolitic water in the channels and bond water coordinated to Mg^{2+} in the octahedral sheet, respectively). The peaks at 1078 and 1028 cm^{-1} are ascribed to the stretching of Si–O(H) bond in the Si–O–Si groups within silica tetrahedral. Peaks at 1429 and 874 cm^{-1} are attributed to the asymmetric and symmetric stretching modes of CO_3^{2-}, respectively; which confirms the presence of carbonate impurity.

On the spectrum of Sep–MW samples, the disappeared characteristic peaks at 1429 and 874 cm^{-1} attributed to impurities, indicated that the sepiolite sample was purified after microwave-assisted acid activation process. Moreover, the intensities of

peaks at 3674 and 3565 cm^{-1} decreased while 3446 and 1642 cm^{-1} increased. This is due to the fact that the microwave-assisted acid activation treatment causes Mg^{2+} in the sepiolite gradually replaced by H^{+} and subsequently Si–OH formed instead.

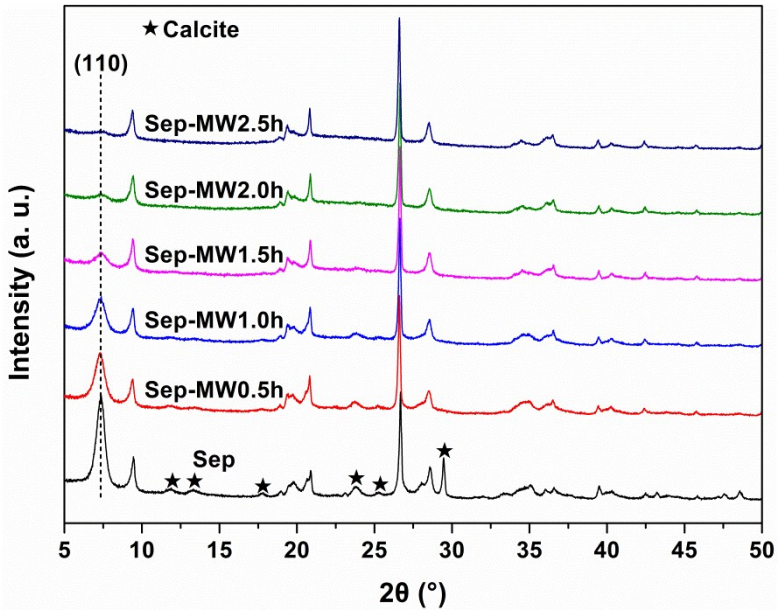

Fig. S2 XRD spectra of Sep and Sep–MW.

In Fig. S2, the strong diffraction peaks at 9.45°, 20.84°, 26.64°, and 28.54° are assigned to sepiolite with an orthorhombic crystalline system. The diffraction at 2θ = 7.32° (the *d*-pacing is 1.21 nm) is related to the (110) plane of the sepiolite lattice. Its intensity gradually decreased and almost disappeared in the samples of Sep–MW2.0h, owing to the effect of defibration which was resulted from the removal of Mg^{2+} in the octahedral structure.

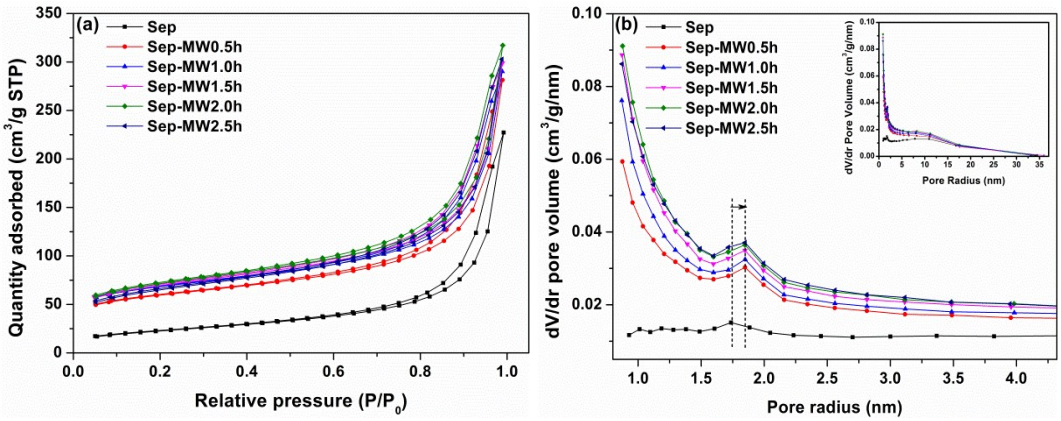

Fig. S3 N_2 adsorption-desorption isotherms (a) and pore size distribution plots (b) of Sep and Sep–MW.

In Fig. S3a, the N_2 adsorption-desorption isotherms of all samples showed a typical IV adsorption isotherm, with a type-H3 hysteresis loop at a relatively wider pressure range (0.9–1.0) which was related to the capillary condensation of half-filled and emptied mesopores in sepiolite. The appearance of type-H3 hysteresis loops showed that the structure of sepiolite with inner channels still maintained after the acid activation treatment with microwave-assisted (F. Franco, et al., *Appl Clay Sci*, 2014, **102**, 15-27). Meanwhile, the Sep–MW samples had higher specific surfaces area and higher porosities, compared with the raw clay mineral (J. Ouyang, et al., *Appl Clay Sci*, 2018, **152**, 267-275). Compared with those of the original sepiolite sample, the meso- and micro-pore volumes of the Sep–MW samples increased markedly, showing an increase in Brunauer-Emmett-Teller (BET) specific surface area and total pore volume while prompting a decrease in average pore diameter.

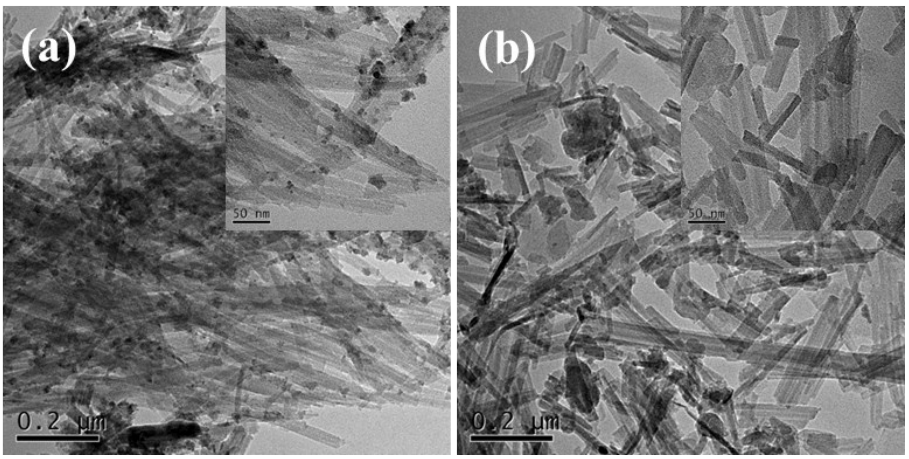

Fig. S4 TEM images of Sep (a) and Sep–MW2.0h (b)

In Fig. S4a, the pristine sepiolite sample exhibits a lump of fibers with a length above 1.0 μm, which were generally assembled in bundles and even form dense aggregates. After microwave-assisted acid treatment, the Sep–MW2.0h sample showed a morphology of well separated fibers with the diameter between 15–20 nm and the length between 200–500 nm, resulting from the extraction of Mg^{2+} during the acid treatment (Z. Feng, et al., *Applied Clay Science*, 2016, **124-125**, 119-126).

Table S1 BET specific surface area, pore volume, Mg^{2+} content and Mg^{2+} removal rate of Sep before and after microwave-assisted acid activation treatment.

Items	Sep	Sep–MW0.5h	Sep–MW1.0h	Sep–MW1.5h	Sep–MW2.0h	Sep–MW2.5h
BET surface area (m^2/g)	81.23	209.49	244.17	247.91	252.88	230.80
t-Plot micropore area (m^2/g)	1.38	81.43	102.31	88.34	87.59	68.92
t-Plot external surface area (m^2/g)	79.85	128.06	141.86	159.57	165.29	161.88
Total pore volume (cm^3/g)	0.0947	0.1714	0.1845	0.2018	0.1979	0.1869
Mg^{2+} content (%)	11.16	10.38	8.89	7.10	6.51	6.11
Mg^{2+} removal rate (%)	–	6.99	20.34	36.38	41.67	45.25

In Table S1, there was 11.16% of the measured Mg^{2+} content in raw sepiolite, which was lower than the theoretical content (e.g. 14.86%), indicated 3.70% impurities (like calcite, marked with the symbol "★" in Fig. S2, completely vanished in Sep–MW2.0h sample). After microwaved-assisted acid activation treatment, the residual Mg^{2+} content was 6.51%, along with the removed Mg^{2+} 41.67%, which was equivalent to those obtained after 8 h with conventional heating methods in our previous work (X. Zhang, et al., *J Membrane Sci*, 2019, **574**, 282-298). The BET specific surface area of sepiolite was 81.23 m^2/g, and that of the Sep–MW2.0h sample increased to 252.88 m^2/g, which was three times higher than that of the raw clay mineral.

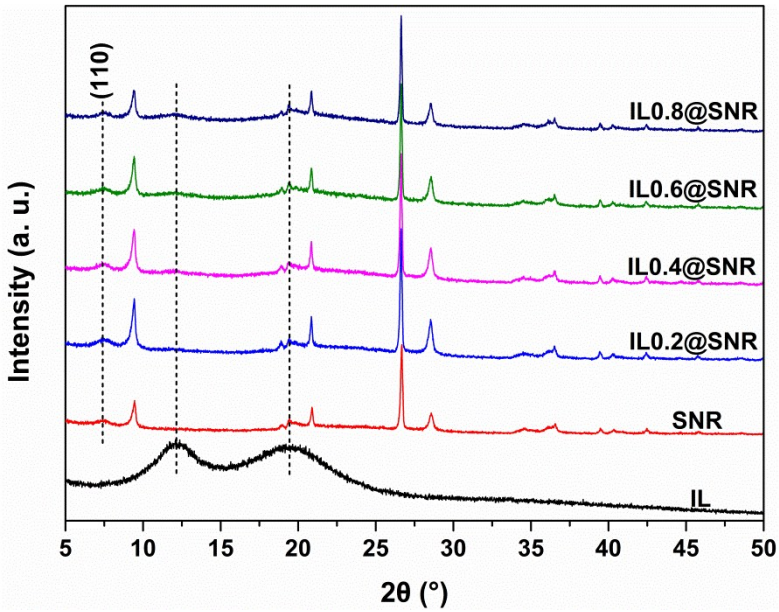

Fig. S5 XRD spectra of IL, SNR, and IL@SNR.

In Fig. S5, all SNR and IL@SNR samples exhibit strongly characteristic peaks of sepiolite particles with an orthorhombic crystalline phase, indicating that the IL@SNR samples maintained the same crystalline structures after IL treatments (J. A. D. Lima, et al., *Appl Clay Sci*, 2017, **143**, 234-240). Two relatively weak and broad peaks at 2θ = 12.09° and 19.38° are corresponded to a characteristic stacking of IL molecules, showing an amorphous or a semi-crystalline structure (A. Triolo, et al., *J Chem Phys*, 2009, **130**, 164532; K. Dong, et al., *Chem Rev*, 2017, **117**, 6636-6695). These two peaks also appeared in the samples IL@SNR, and increased in intensity with an increasing of IL content, confirming their existence in IL@SNR samples.

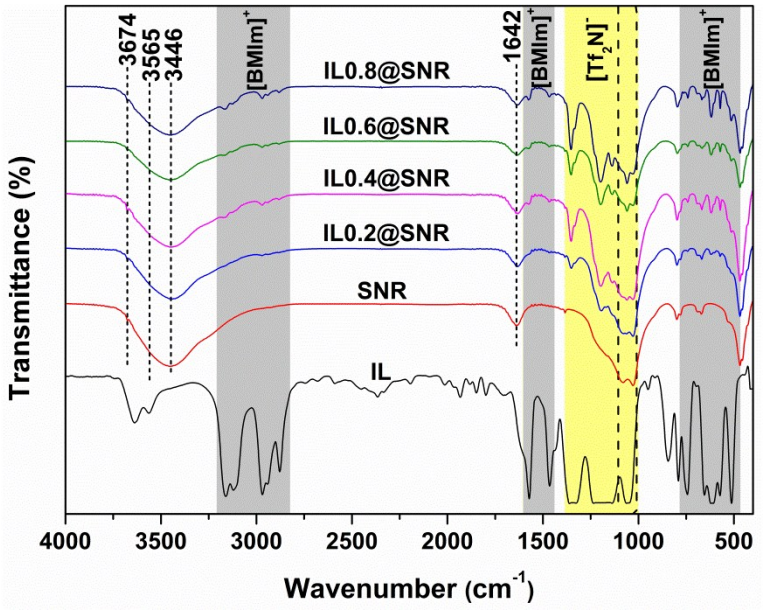

Fig. S6 FTIR spectra of IL, SNR, and IL@SNR.

In Fig. S6, the characteristic IR spectra of $[BMIm]^+$ and $[Tf_2N]^-$ were more obvious with the increasing amount of ILs loading. A broad peak in the range of 4000–3000 cm^{-1} represents the crystal water existed in the inner tunnels of SNRs. The decrease in intensity of this peak in IL@SNR samples indicated the partial removal of crystal water, which was replaced by encapsulated ILs (J. A. D. Lima, et al., *Appl Clay Sci*, 2017, **143**, 234-240). The new bands appearing at 1352, 1332, 1195, and 1060 cm^{-1} are attributed to the characteristic peak of the anion $[Tf_2N]^-$. The bands at 3171 and 3126 cm^{-1} as well as 1576, 741, 618 and 571 cm^{-1} are attributed to the C–H stretching and in-plane bending vibration on the imidazole ring, skeleton and bending vibration of the imidazole ring, respectively, in the cationic $[BMIm]^+$. Meanwhile, the C–H symmetric, asymmetric stretching vibration and in-plane bending vibration of alkyl substituent on the imidazole ring are located at 2986, 2924, 2853 and 1467 cm^{-1}, respectively.

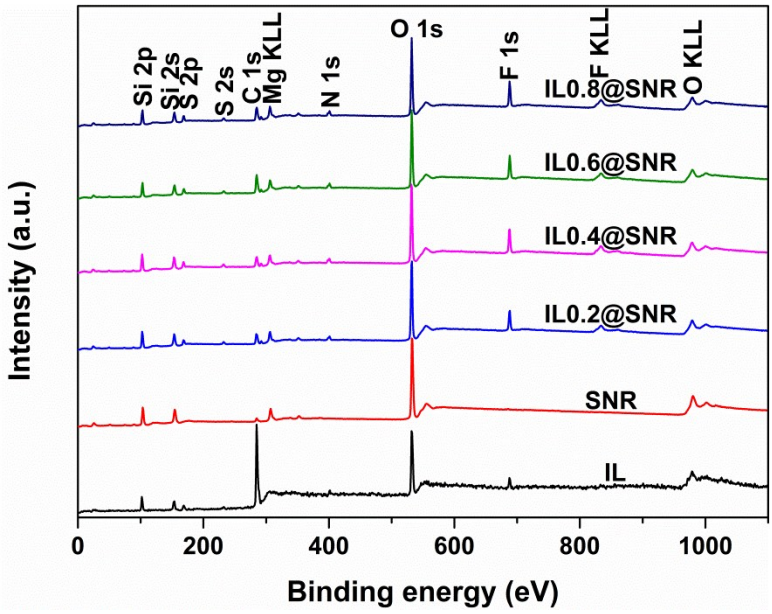

Fig. S7 XPS spectra of IL, SNR, and IL@SNR.

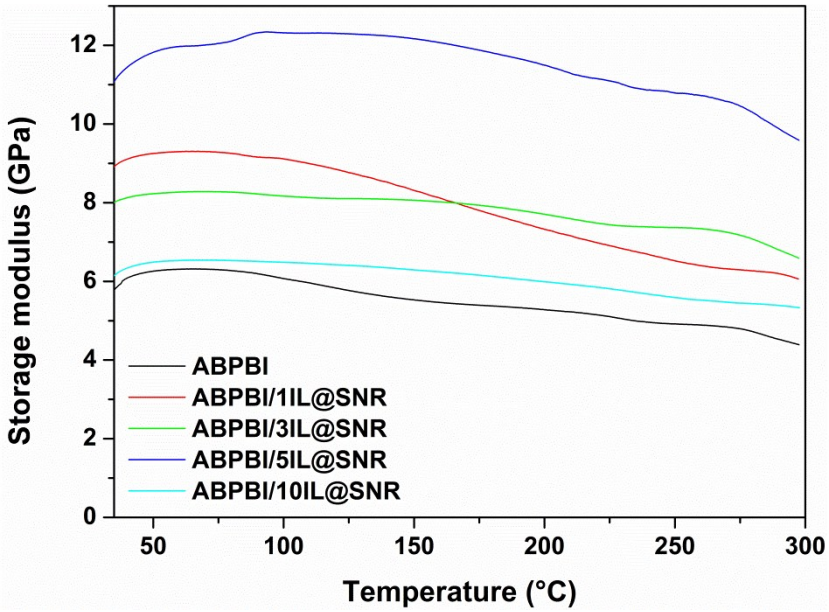

Fig. S8 DMA plots of ABPBI and ABPBI/IL@SNR composite membranes.

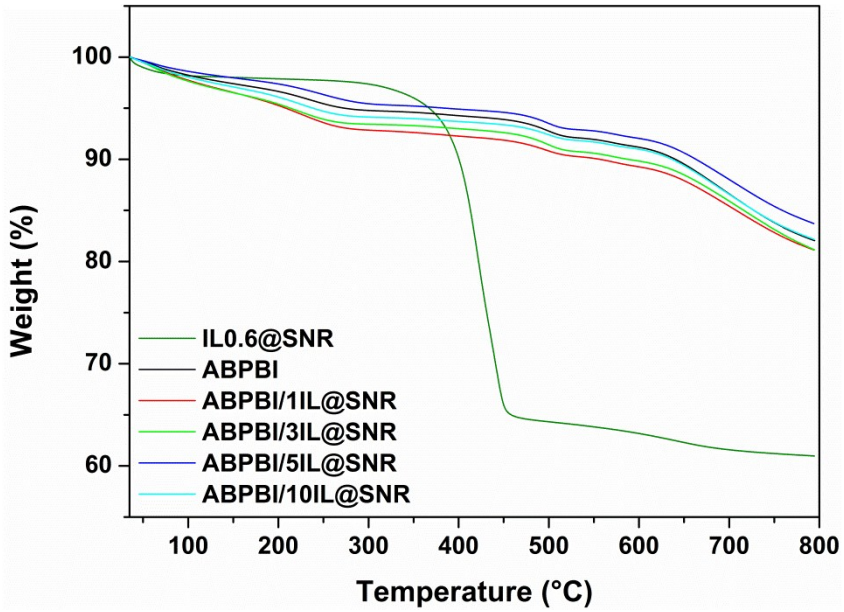

Fig. S9 TGA plots of IL0.6@SNR, ABPBI and ABPBI/IL@SNR composite membranes.

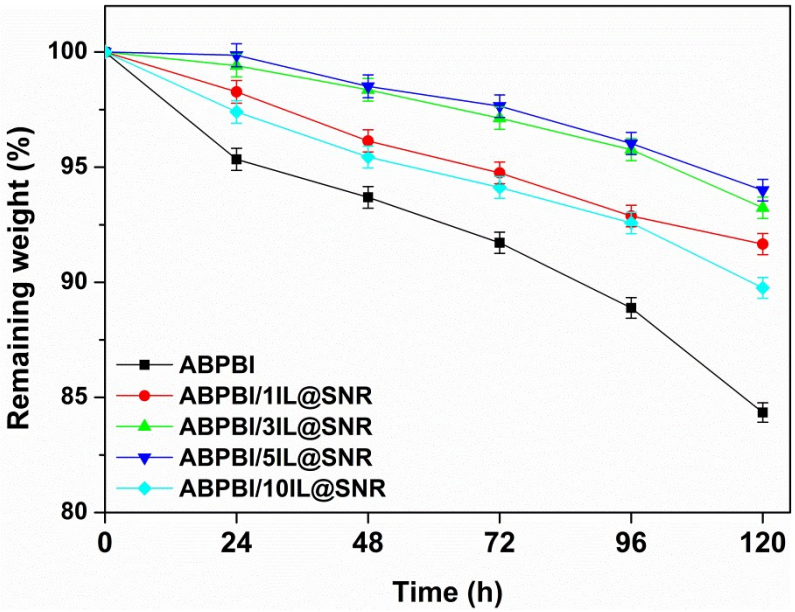

Fig. S10 Oxidative stability plots of ABPBI and ABPBI/IL@SNR composite membranes.

Table S2 Thermo-mechanical data, tensile strength, elongation at break, and modulus of pristine ABPBI membrane and ABPBI/IL@SNR composite membranes obtained by DMA and tensile testing.

Samples	E' (GPa)				Tensile strength	Elongation at break	Modulus
	25 °C	100 °C	200 °C	300 °C	(MPa)	(%)	(GPa)
ABPBI	5.77	6.07	5.28	4.39	132.67±6.2	42.58±5.8	2.71±0.12
ABPBI/1IL@SNR	8.92	9.11	7.32	6.06	180.01±6.7	38.99±4.0	3.35±0..08
ABPBI/3IL@SNR	8.02	8.17	7.70	6.59	192.95±4.9	32.92±3.8	3.99±0.07
ABPBI/5IL@SNR	11.10	12.32	11.49	9.59	204.24±4.6	27.75±4.2	3.98±0.09
ABPBI/10IL@SNR	6.15	6.49	5.99	5.33	166.19±5.6	26.94±5.1	3.14±0.11

Table S3 Thickness and E_a of PA doped ABPBI and ABPBI/IL@SNR composite membranes.

Samples	Thickness (μm)	E_a (kJ/mol)			
		0% RH	20% RH	60% RH	98% RH
ABPBI–1.66PA	67	38.73	37.57	32.58	18.13
ABPBI/1IL@SNR–1.72PA	59	27.58	24.21	18.86	10.28
ABPBI/3IL@SNR–1.81PA	58	23.59	19.22	14.85	9.01
ABPBI/5IL@SNR–1.93PA	56	22.95	18.61	13.90	5.47
ABPBI/10IL@SNR–1.71PA	63	33.82	30.45	24.80	14.91
Nafion 212	50	–	–	13.22	10.73